Neutron star matter based on a parity doublet model including the $a_0(980)$ meson

Yuk Kei Kong [*] and Takuya Minamikawa [†]
Department of Physics, Nagoya University, Nagoya 464-8602, Japan

Masayasu Harada [‡]
Department of Physics, Nagoya University, Nagoya 464-8602, Japan;
Kobayashi-Maskawa Institute for the Origin of Particles and the Universe, Nagoya University, Nagoya, 464-8602, Japan;
and Advanced Science Research Center, Japan Atomic Energy Agency, Tokai 319-1195, Japan

(Received 24 June 2023; revised 8 September 2023; accepted 11 October 2023; published 22 November 2023)

We study the effect of the isovector-scalar meson $a_0(980)$ on the properties of nuclear matter and the neutron star (NS) matter by constructing a parity doublet model with including the a_0 meson based on the chiral $SU(2)_L \times SU(2)_R$ symmetry. We also include the ω-ρ mixing contribution to adjust the slope parameter at the saturation. We find that, when the chiral invariant mass of nucleon m_0 is smaller than about 800 MeV, the existence of $a_0(980)$ enlarges the symmetry energy by strengthening the repulsive ρ meson coupling. On the other hand, for large m_0 where the Yukawa coupling of $a_0(980)$ to nucleon is small, the symmetry energy is reduced by the effect of ω-ρ mixing. We then construct the equation of state (EoS) of a neutron star matter to obtain the mass-radius relation of NS. We find that, in most choices of m_0, the existence of $a_0(980)$ stiffens the EoS and makes the radius of NS larger. We then constrain the chiral invariant mass of nucleon from the observational data of NS, and find that $580\ \text{MeV} \lesssim m_0 \lesssim 860\ \text{MeV}$ for $L_0 = 57.7$ MeV.

DOI: 10.1103/PhysRevC.108.055206

I. INTRODUCTION

Spontaneous chiral symmetry breaking is one of the most important properties in the low-energy hadron physics, which is expected to generate a part of hadron masses and cause the mass difference between chiral partners. In particular, it is interesting to study the origin of nucleon mass in terms of the chiral symmetry structure.

In the traditional linear σ model, the entire nucleon mass is generated from the spontaneous chiral symmetry breaking, in which the chiral partner to the ordinary nucleon is the nucleon itself. In the parity doublet model (PDM) proposed in Ref. [1], on the other hand, an excited nucleon such as $N(1535)$ is regarded as the chiral partner to ordinary nucleon. The spontaneous symmetry breaking generates the mass difference between them. If the chiral symmetry was not broken, their masses would be degenerated into, so called, the chiral invariant mass m_0. The existence of the chiral invariant mass and its possible relation to the parity doubling structure is also supported by the lattice quantum chromodynamics (QCD) simulation [2,3]. In addition, recent analysis based on the QCD sum rules [4] also supports the existence which suggest that the origin of the chiral invariant mass is the gluon condensate. Therefore, quantitative and qualitative study of the chiral invariant mass will help us to understand the origin of hadron masses.

There are several analyses to determine the value of m_0 by studying the nucleon properties at vacuum. For example, the analysis in Ref. [5] shows that m_0 is smaller than 500 MeV using the decay width of $N(1535)$, while Ref. [6] includes higher derivative interaction which makes the large m_0 consistent with the decay width.

The chiral symmetry is expected to be partially restored in the high density region, study of which will provide some information on the chiral invariant mass. Actually, the PDM is applied to study the high density matter in several analyses such as in Refs. [7–39]. Recently in Refs. [33,35,37,38], the equation of state (EoS) of neutron star (NS) matter constructed from an extended PDM [19] was connected to the one from the NJL-type quark model following Refs. [40,41]. The analysis of Ref. [33] use the observational data of NS given in Refs. [42–47] to put constraint to the chiral invariant mass m_0 as $600\ \text{MeV} \lesssim m_0 \lesssim 900\ \text{MeV}$, which was updated in Refs. [37,38] to $400\ \text{MeV} \lesssim m_0 \lesssim 700\ \text{MeV}$ by considering the effect of anomaly as well as new data analysis [48–50].

In recent decades, increasing attention has been paid to the effect of isovector-scalar $a_0(980)$ meson (or called δ meson) on asymmetric matter such as NS because it is expected to provide a different effect to neutrons and protons. References [51–61] use Walecka-type relativistic mean-field (RMF) models, and Refs. [62,63] use density-dependent RMF models to study the effect of $a_0(980)$ meson to the symmetry energy as well as to the EoS of asymmetric matter. It was pointed that the existence of the a_0 meson increases the symmetry

*yukkekong2-c@hken.phys.nagoya-u.ac.jp
†minamikawa@hken.phys.nagoya-u.ac.jp
‡harada@hken.phys.nagoya-u.ac.jp

energy [51,53,54,57–61], and that it stiffens the NS EoS [52–54,56,57] and asymmetric matter EoS [63]. Since there is no study on the effect of a_0 meson to the matter properties in PDM to our best knowledge, we study the effect of a_0 meson in the PDM to the symmetry energy and NS properties.

In this work, we construct a PDM with including the $a_0(980)$ meson based on the chiral $SU(2)_L \times SU(2)_R$ symmetry. We first study the effect of a_0 meson to the symmetry energy for several choices of given values of the chiral invariant mass m_0. We will show that the symmetry energy is enhanced for most choices of m_0, but is reduced for $m_0 = 900$ MeV. We then obtain the EoS of NS matter to compute the M-R relation of NS. We think that it is not suitable to use the present hadronic model in the high density region of the NS since the model includes only a nucleon and its chiral partner for baryons, while it is expected that the strangeness may appear in the high density region. Thus, in the present analysis, we adopt a crossover prescription proposed in Ref. [40] to construct a unified EoS by interpolating an Nambu–Jona-Lasinio (NJL)-type quark model with the EoS from the PDM as done in Ref. [33]. By comparing the resultant M-R relation to the observational data of NS, we obtain the constraint to the chiral invariant mass as 580 MeV $\lesssim m_0 \lesssim$ 860 MeV for $L_0 = 57.7$ MeV.

This work is organized as follows. We describe our parity doublet model in Sec. II. Then, we construct the hadronic EoS under the mean-field approximation in Sec. III. In Sec. IV, we compute the symmetry energy and study the effect of $a_0(980)$ on it. In Sec. V, we construct the neutron star EoS by interpolating the EoS for hadronic matter with the EoS of quark matter from the NJL-type quark model, and compute the M-R relation. We then study the impact of $a_0(980)$ meson on neutron star EoS as well as the M-R relation. Furthermore, we compare the results to the observational data of the neutron star and give a constraint to the chiral invariant mass of the nucleon. Finally, this work is summarized in Sec. VI.

II. FORMALISM

A. Parity doublet model with isovector scalar meson

To study the $a_0(980)$ effect, we construct an $SU(2)_L \times SU(2)_R$ parity doublet model. The effective Lagrangian is given by

$$\mathcal{L} = \mathcal{L}_N + \mathcal{L}_M + \mathcal{L}_V \,, \tag{1}$$

where the Lagrangian is separated into three parts: the nucleon Lagrangian $\mathcal{L}_N$, the scalar meson Lagrangian $\mathcal{L}_M$, and the vector meson Lagrangian $\mathcal{L}_V$. In $\mathcal{L}_M$, the scalar meson field M is introduced as the $(2,2)_{-2}$ representation under the $SU(2)_L \times SU(2)_R \times U(1)_A$ symmetry which transforms as

$$M \to e^{-2i\theta_A} g_L M g_R^\dagger \,, \tag{2}$$

where $g_{R,L} \in SU(2)_{R,L}$ and $e^{-2i\theta_A} \in U(1)_A$. We parametrize M as

$$M = [\sigma + i\vec{\pi}\cdot\vec{\tau}] - [\vec{a}_0\cdot\vec{\tau} + i\eta], \tag{3}$$

where $\sigma, \vec{\pi}, \vec{a}_0, \eta$ are scalar meson fields, $\vec{\tau}$ are the Pauli matrices. Notice that the vacuum expectation value (VEV) of M is

$$\langle 0|M|0\rangle = \begin{pmatrix} \sigma_0 & 0 \\ 0 & \sigma_0 \end{pmatrix}, \tag{4}$$

where $\sigma_0 = \langle 0|\sigma|0\rangle$ is the VEV of the σ field. The explicit form of the Lagrangian $\mathcal{L}_M$ is given by

$$\mathcal{L}_M = \tfrac{1}{4}\mathrm{tr}[\partial_\mu M \partial^\mu M^\dagger] - V_M \,, \tag{5}$$

where V_M is the potential for M. In the present model, V_M is taken as

$$\begin{aligned} V_M = &-\frac{\bar{\mu}^2}{4}\mathrm{tr}[M^\dagger M] + \frac{\lambda_{41}}{8}\mathrm{tr}[(M^\dagger M)^2] \\ &-\frac{\lambda_{42}}{16}\{\mathrm{tr}[M^\dagger M]\}^2 - \frac{\lambda_{61}}{12}\mathrm{tr}[(M^\dagger M)^3] \\ &-\frac{\lambda_{62}}{24}\mathrm{tr}[(M^\dagger M)^2]\mathrm{tr}[M^\dagger M] - \frac{\lambda_{63}}{48}\{\mathrm{tr}[M^\dagger M]\}^3 \\ &-\frac{m_\pi^2 f_\pi}{4}\mathrm{tr}[M + M^\dagger] - \frac{K}{8}\{\det M + \det M^\dagger\} \,. \end{aligned} \tag{6}$$

In the above potential, the first three terms account for the most general possible terms that are invariant under $SU(2)_L \times SU(2)_R \times U(1)_A$ symmetry with the mass dimension less than or equal to four. The terms with the coefficients λ_{61}, λ_{62}, and λ_{63} are the six-point interaction terms for σ field that were introduced in Ref. [19] to reproduce the nuclear saturation properties. We note that all possible six-point interactions are included here. In the large N_c expansion of QCD, these terms are counted as $\mathrm{tr}[(M^\dagger M)^3] \sim O(N_c)$, $\mathrm{tr}[(M^\dagger M)^2]\mathrm{tr}[M^\dagger M] \sim O(1)$, and $\{\mathrm{tr}[M^\dagger M]\}^3 \sim O(1/N_c)$. Therefore, the latter two terms are suppressed compared with the first one. In this work, we first study the effect of the $a_0(980)$ meson with only the leading order term, and then study the effect of these higher order interactions to the symmetry energy and neutron star properties. The seventh term in V_M is the explicit symmetry-breaking term due to the nonzero current quark masses, which explicitly breaks the $SU(2)_L \times SU(2)_R \times U(1)_A$ symmetry. The last term is introduced to account for the $U(1)_A$ anomaly. Therefore, $\mathcal{L}_M$ is $SU(2)_L \times SU(2)_R \times U(1)_A$ invariant except the last two terms of V_M. For the vector meson, the isotriplet ρ meson and isosinglet ω meson are included using the hidden local symmetry [64,65] to account for the repulsive force in the matter.

Finally, the baryonic Lagrangian $\mathcal{L}_N$ based on the parity doubling structure [1,5] is given by

$$\begin{aligned} \mathcal{L}_N = &\bar{N}_1 i\partial\!\!\!/ N_1 + \bar{N}_2 i\partial\!\!\!/ N_2 - m_0[\bar{N}_1\gamma_5 N_2 - \bar{N}_2\gamma_5 N_1] \\ &- g_1[\bar{N}_{1l} M N_{1r} + \bar{N}_{1r} M^\dagger N_{1l}] \\ &- g_2[\bar{N}_{2r} M N_{2l} + \bar{N}_{2l} M^\dagger N_{2r}], \end{aligned} \tag{7}$$

where $N_{ir}(N_{il})$ $(i = 1, 2)$ is the right-handed (left-handed) component of the nucleon fields N_i. By diagonalizing $\mathcal{L}_N$, we obtain two baryon fields N_+ and N_- corresponding to the positive parity and negative parity nucleon fields, respectively. Their masses at vacuum are obtained as [1,5]

$$m_\pm^{(\mathrm{vac})} = \tfrac{1}{2}\Big[\sqrt{(g_1+g_2)^2\sigma_0^2 + 4m_0^2} \pm (g_1 - g_2)\sigma_0\Big] \,. \tag{8}$$

In the present work, N_+ and N_- are identified as $N(939)$ and $N(1535)$, respectively, so that m_+ (m_-) is the mass of $N(939)$ [$N(1535)$].

III. NUCLEAR MATTER AT NONZERO DENSITY

A. Mean field approximation

To construct the nuclear matter from the model introduced in the previous section, we adopt the mean-field approximation following [33,37], by taking

$$\sigma(x) \to \sigma, \quad \pi(x) \to 0, \quad \eta(x) \to 0. \tag{9}$$

The $a_0(980)$ mean field is assumed to have nonzero value only in the third axis of isospin as

$$a_0^i(x) \to a\,\delta_{i3}\,. \tag{10}$$

Thus, the mean field for M becomes

$$\langle M\rangle = \begin{pmatrix} \sigma - a & 0 \\ 0 & \sigma + a \end{pmatrix}. \tag{11}$$

Notice that the mean field of $a_0(980)$ vanishes ($a = 0$) in the symmetric nuclear matter as well as vacuum, due to the isospin invariance.

Redefining the parameters as

$$\begin{aligned} \bar\mu_\sigma^2 &\equiv \bar\mu^2 + \tfrac{1}{2}K,\\ \bar\mu_a^2 &\equiv \bar\mu^2 - \tfrac{1}{2}K = \bar\mu_\sigma^2 - K,\\ \lambda_4 &\equiv \lambda_{41} - \lambda_{42},\\ \gamma_4 &\equiv 3\lambda_{41} - \lambda_{42},\\ \lambda_6 &\equiv \lambda_{61} + \lambda_{62} + \lambda_{63},\\ \lambda_6' &\equiv \tfrac{4}{3}\lambda_{62} + 2\lambda_{63}, \end{aligned} \tag{12}$$

we write V_M in terms of the meson mean fields as

$$\begin{aligned} V_M = &-\frac{\bar\mu_\sigma^2}{2}\sigma^2 - \frac{\bar\mu_a^2}{2}a^2 + \frac{\lambda_4}{4}(\sigma^4 + a^4) + \frac{\gamma_4}{2}\sigma^2 a^2\\ &- \frac{\lambda_6}{6}(\sigma^6 + 15\sigma^2 a^4 + 15\sigma^4 a^2 + a^6)\\ &+ \lambda_6'(\sigma^2 a^4 + \sigma^4 a^2)\\ &- m_\pi^2 f_\pi \sigma. \end{aligned} \tag{13}$$

We note that λ_6' is of subleading order in the large N_c expansion.

In the mean-field approximation, the vector meson fields are taken as

$$\omega_\mu(x) \to \omega\delta_{\mu 0}, \quad \rho_\mu^i(x) \to \rho\delta_{\mu 0}\delta_{i3}. \tag{14}$$

The Lagrangian $\mathcal{L}_V$ of the vector mesons can then be written in terms of the mean fields of the vector mesons as

$$\begin{aligned} \mathcal{L}_V = &-g_\omega \sum_{\alpha j} \bar N_{\alpha j}\gamma^0 \omega N_{\alpha j} - g_\rho \sum_{\alpha j} \bar N_{\alpha j}\gamma^0 \frac{\tau_3}{2}\rho N_{\alpha j}\\ &+ \frac{1}{2}m_\omega^2\omega^2 + \frac{1}{2}m_\rho^2\rho^2 + \lambda_{\omega\rho} g_\omega^2 g_\rho^2 \omega^2\rho^2. \end{aligned} \tag{15}$$

We note that the ω-ρ mixing is included in our model to reduce the slope parameter following Ref. [37].

Here, we show that $\lambda_{\omega\rho} > 0$ is required in the present model. The vector meson potential is written as

$$V_V \equiv -\tfrac{1}{2}m_\omega^2\omega^2 - \tfrac{1}{2}m_\rho^2\rho^2 - \lambda_{\omega\rho} g_\omega^2 g_\rho^2 \omega^2\rho^2. \tag{16}$$

The vacuum expectation values of the vector meson fields are chosen at the stationary point of the potential V_V. The stationary conditions,

$$\begin{aligned} \frac{\partial V_V}{\partial \omega} &= \omega\big[m_\omega^2 + 2\lambda_{\omega\rho} g_\omega^2 g_\rho^2 \rho^2\big] = 0\,,\\ \frac{\partial V_V}{\partial \rho} &= \rho\big[m_\rho^2 + 2\lambda_{\omega\rho} g_\omega^2 g_\rho^2 \omega^2\big] = 0\,, \end{aligned} \tag{17}$$

imply that there are two stationary points

$$(\omega^2, \rho^2) = (0,0), \left(-\frac{m_\rho^2}{2\lambda_{\omega\rho} g_\omega^2 g_\rho^2}, -\frac{m_\omega^2}{2\lambda_{\omega\rho} g_\omega^2 g_\rho^2} \right), \tag{18}$$

which give the potential as

$$V_V = \begin{cases} 0, & \text{for } (\omega^2, \rho^2) = (0,0)\,,\\ \frac{m_\omega^2 m_\rho^2}{4\lambda_{\omega\rho} g_\omega^2 g_\rho^2}, & \text{for } (\omega^2, \rho^2) = \left(-\frac{m_\rho^2}{2\lambda_{\omega\rho} g_\omega^2 g_\rho^2}, -\frac{m_\omega^2}{2\lambda_{\omega\rho} g_\omega^2 g_\rho^2} \right). \end{cases} \tag{19}$$

In the present work, vanishing vacuum expectation values of the vector meson fields are required at zero density due to the Lorentz-invariance of the vacuum. Therefore, we need $\lambda_{\omega\rho} > 0$ such that $(\omega^2, \rho^2) = (0,0)$ minimizes the effective potential V_V at vacuum.

Now, the thermodynamic potential for the nucleons is written as

$$\Omega_N = -2 \sum_{\alpha=\pm,\, j=p,n} \int^{k_f} \frac{d^3p}{(2\pi)^3}[\mu_j^* - \omega_{\alpha j}], \tag{20}$$

where $\alpha = \pm$ denotes the parity and $j = p, n$ the isospin of nucleons. μ_j^* is the effective chemical potential given by

$$\mu_j^* \equiv (\mu_B - g_\omega\omega) + \frac{j}{2}(\mu_I - g_\rho\rho)\,, \tag{21}$$

and $\omega_{\alpha j}$ is the energy of the nucleon defined as $\omega_{\alpha j} = \sqrt{(\vec p)^2 + (m_{\alpha j}^*)^2}$, where $\vec p$ and $m_{\alpha j}^*$ are the momentum and the effective mass of the nucleon. The effective mass $m_{\alpha j}^*$ is given by

$$\begin{aligned} m_{\alpha j}^* = \tfrac{1}{2}\Big[&\sqrt{(g_1+g_2)^2(\sigma - ja)^2 + 4m_0^2}\\ &+ \alpha(g_1 - g_2)(\sigma - ja)\Big]. \end{aligned} \tag{22}$$

Notice that the masses of proton and neutron become nondegenerate in the asymmetric matter due to the nonzero mean field of $a_0(980)$.

The entire thermodynamic potential for hadronic matter is expressed as

$$\begin{aligned} \Omega_H = \Omega_N &- \frac{\bar\mu_\sigma^2}{2}\sigma^2 - \frac{\bar\mu_a^2}{2}a^2 + \frac{\lambda_4}{4}(\sigma^4 + a^4) + \frac{\gamma_4}{2}\sigma^2 a^2\\ &- \frac{\lambda_6}{6}(\sigma^6 + 15\sigma^2 a^4 + 15\sigma^4 a^2 + a^6) + \lambda_6'(\sigma^2 a^4 + \sigma^4 a^2)\\ &- m_\pi^2 f_\pi\sigma - \frac{1}{2}m_\omega^2\omega^2 - \frac{1}{2}m_\rho^2\rho^2 - \lambda_{\omega\rho} g_\omega^2 g_\rho^2\omega^2\rho^2 - \Omega_0, \end{aligned} \tag{23}$$

TABLE I. Values of g_1, g_2, $\bar{\mu}_\sigma^2$, λ_4, λ_6, g_ω for $m_0 = 500$–900 MeV.

m_0 (MeV)	500	600	700	800	900
g_1	9.02	8.48	7.81	6.99	5.96
g_2	15.47	14.93	14.26	13.44	12.41
$\bar{\mu}_\sigma^2/f_\pi^2$	22.70	22.35	19.28	11.93	1.50
λ_4	41.94	40.39	35.46	23.12	4.43
$\lambda_6 f_\pi^2$	16.94	15.75	13.89	8.89	0.64
g_ω	11.34	9.13	7.30	5.66	3.52
$\bar{\mu}_a^2/f_\pi^2$	−10.43	−10.79	−13.86	−21.21	−31.64
γ_4	191.41	185.07	172.70	140.38	88.67

where we subtracted the potential at the vacuum

$$\Omega_0 \equiv -\frac{\bar{\mu}_\sigma^2}{2} f_\pi^2 + \frac{\lambda_4}{4} f_\pi^4 - \frac{\lambda_6}{6} f_\pi^6 - m_\pi^2 f_\pi^2. \tag{24}$$

B. Parameters determination

In the present model, there are 12 parameters to be determined for a given value of the chiral invariant mass m_0:

$$g_1, g_2, \bar{\mu}_\sigma^2, \bar{\mu}_a^2, \lambda_4, \gamma_4, \lambda_6, \lambda_6', g_\omega, g_\rho, \lambda_{\omega\rho}. \tag{25}$$

We determine them from the vacuum properties as well as nuclear saturation properties as follows:

The vacuum expectation value of σ is taken to be $\sigma_0 = f_\pi$ with the pion decay constant $f_\pi = 92.4$ MeV. The Yukawa coupling constants g_1 and g_2 are determined by fitting them to the nucleon masses at vacuum given by Eq. (8), with $m_+ = m_N = 939$ MeV and $m_- = m_{N^*} = 1535$ MeV. The value of g_1, g_2 is given in Table I. It is convenient to define the effective Yukawa couplings of σ and $a_0(980)$ as

$$\begin{aligned} g_{\sigma N_{\alpha j} N_{\alpha j}} &\equiv \left.\frac{\partial m_{\alpha j}^*}{\partial \sigma}\right|_{\text{vacuum}} \\ &= \frac{1}{2}\left[\frac{(g_1+g_2)^2 f_\pi}{\sqrt{(g_1+g_2)^2 f_\pi^2 + 4m_0^2}} + \alpha(g_1 - g_2)\right], \end{aligned} \tag{26}$$

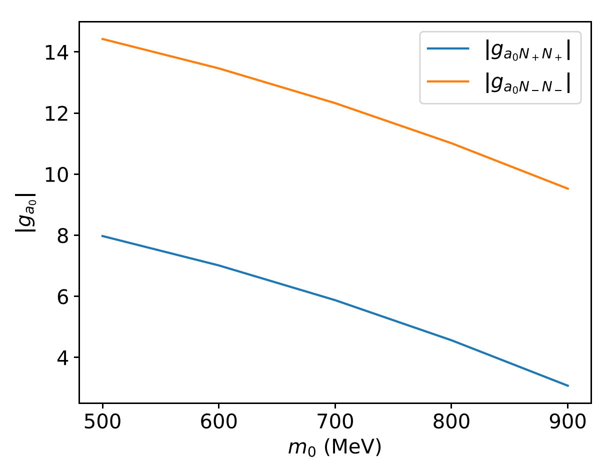

FIG. 1. Strength of the Yukawa couplings of a_0 meson, $|g_{a_0NN}| = |g_{\sigma NN}|$, as a function of the chiral invariant mass m_0.

TABLE II. Saturation properties that are used to determine the model parameters: saturation density n_0, binding energy B_0, incompressibility K_0, symmetry energy S_0, and slope parameter L_0.

n_0 [fm^{-3}]	B_0 [MeV]	K_0 [MeV]	S_0 [MeV]	L_0 [MeV]
0.16	16	240	31	40–80

$$g_{a_0 N_{\alpha j} N_{\alpha j}} \equiv \left.\frac{\partial m_{\alpha j}^*}{\partial a}\right|_{\text{vacuum}} = (-j) g_{\sigma N_{\alpha j} N_{\alpha j}} . \tag{27}$$

These imply that σ and $a_0(980)$ meson couple to the nucleons with the same strength $|g_{\sigma NN}| = |g_{a_0 NN}|$. In Fig. 1 we show how the the Yukawa coupling of a_0 meson changes as m_0 changes, which shows that the Yukawa coupling of a_0 meson decreases as m_0 increases. Then, the a_0 meson effect to the symmetry energy becomes smaller for large m_0 as we will show later.

Tables I also shows the parameters $\bar{\mu}_\sigma^2$, λ_4, λ_6, g_ω that are determined from the constraints at nuclear saturation. The saturation properties used are summarized in Table II. Then, $\bar{\mu}_a^2 = \bar{\mu}_\sigma^2 - K$ is determined from K given by

$$K = m_\eta^2 - m_\pi^2 . \tag{28}$$

Similarly, γ_4 is given by

$$\gamma_4 = \frac{m_a^2 + 5\lambda_6 f_\pi^4 + \bar{\mu}_a^2}{f_\pi^2} , \tag{29}$$

from the mass of $a_0(980)$. We summarize the values of masses of mesons in Table III.

In the present analysis, λ_6' is treated as a free parameter to study the high-order effect in the large N_c expansion to the mesonic six-point interactions. Since the λ_6' term is suppressed by $1/N_c$ compared with the λ_6 term in the large N_c expansion, we assume that $|\lambda_6'| \lesssim |\lambda_6|$ is satisfied, and take $\lambda_6' = 0, \pm\lambda_6$ to examine the effect of the higher order six-point interactions to the symmetry energy and neutron star properties.

Tables IV and V show the values of the parameters g_ρ and $\lambda_{\omega\rho}$ that are determined from fitting S_0 and L_0 with $\lambda_6' = 0$. As we will discuss later, the higher-order effect is small and the values of g_ρ and $\lambda_{\omega\rho}$ are similar for $\lambda_6' = \pm\lambda_6$. We note that the inclusion of the ω-ρ mixing allows us to vary the slope parameter L_0 in the present model. Reference [66] shows that $L_0 = 57.7 \pm 19$ MeV, so we take $L_0 = 40 - 80$ MeV as the physical input to compare the effect of $a_0(980)$.

To compare how the matter properties are affected by $a_0(980)$ meson, we eliminate the $a_0(980)$ meson by taking the mean field $a = 0$ in the potential (23) and the masses in Eq. (22). The parameters are determined by fitting them to nuclear saturation properties and vacuum properties. Similarly, in the model without $a_0(980)$, the model parameters

TABLE III. Values of meson masses at vacuum in unit of MeV.

π	$a_0(980)$	η	ω	ρ
140	980	550	783	776

TABLE IV. g_ρ of model with $a_0(980)$ meson and $\lambda_6' = 0$.

m_0 (MeV)	500	600	700	800	900
$L_0 = 40$ MeV	19.43	15.52	13.89	12.64	11.40
$L_0 = 50$ MeV	18.75	15.03	13.35	12.0	10.69
$L_0 = 60$ MeV	18.14	14.59	12.87	11.45	10.09
$L_0 = 70$ MeV	17.58	14.18	12.44	10.97	9.59
$L_0 = 80$ MeV	17.07	13.81	12.05	10.54	9.15

TABLE VI. g_ρ of model without $a_0(980)$ meson.

m_0 (MeV)	500	600	700	800	900
$L_0 = 40$ MeV	12.48	10.99	10.72	10.64	10.61
$L_0 = 50$ MeV	10.72	10.01	9.91	9.90	9.91
$L_0 = 60$ MeV	9.54	9.24	9.25	9.29	9.34
$L_0 = 70$ MeV	8.68	8.63	8.71	8.78	8.86
$L_0 = 80$ MeV	8.02	8.13	8.26	8.35	8.44

$g_1, g_2, \bar{\mu}_\sigma^2, \lambda_4, \lambda_6$ are the same as in the $a_0(980)$ model, since these parameters are determined from the properties of symmetric matter irrelevant for isospin asymmetry. We notice that γ_4 and λ_6' terms do not exist in the model without $a_0(980)$ which takes account of the cross interactions between σ and a. We summarize the values of the parameters g_ρ and $\lambda_{\omega\rho}$ in the model without the a_0 meson in Tables VI and VII.

IV. EFFECT OF a_0(980) TO THE SYMMETRY ENERGY

In this section, we study the effect of $a_0(980)$ meson to the symmetry energy. For a while we take $\lambda_6' = 0$, and study its effect by taking $\lambda_6' = \pm\lambda_6$ at the end of this section. In the present model, the symmetry energy S(n_B) for a given density n_B is expressed as

$$\begin{aligned} S(n_B) &= \frac{n_B}{8}\frac{\partial \mu_I}{\partial n_I}\bigg|_{n_I=0} \\ &= \frac{(k_+^*)^2}{6\mu_+^*} + \frac{n_B}{2}\frac{(g_\rho/2)^2}{m_\rho^2 + \left(2\lambda_{\omega\rho}g_\omega^4 g_\rho^2 n_B^2/m_\omega^4\right)} \\ &\quad - \frac{n_B}{4}\frac{m_+^*}{\mu_+^*}\frac{\partial m_{+n}^*}{\partial n_I}\bigg|_{n_I=0}, \end{aligned} \tag{30}$$

where $\mu_+^* \equiv \mu_p^*|_{n_I=0} = \mu_n^*|_{n_I=0}$ is the effective chemical potential for $N(939)$ in the symmetric matter, $k_+^* \equiv \sqrt{(\mu_p^*)^2 - (m_{+p}^*)^2}|_{n_I=0} = \sqrt{(\mu_n^*)^2 - (m_{+n}^*)^2}|_{n_I=0}$ the corresponding Fermi momentum, $m_+^* \equiv m_{+p}^*|_{n_I=0} = m_{+n}^*|_{n_I=0}$ the mass. Figure 2 shows the symmetry energy for $m_0 =$ 500–900 MeV and $L_0 =$ 40–80 MeV. Here, we compare the results obtained with and without the existence of the $a_0(980)$ meson. We observe that, in most cases, the symmetry energy is stiffened by the existence of $a_0(980)$ and the difference of the symmetry energy between the models with same L_0 is larger for smaller m_0. At $n_B = 2n_0$, the symmetry energy $S(2n_0)$ is enlarged by as large as 51% in the a_0 model depending on the input parameters.

To further understand the nature of this stiffening of the symmetry energy in the $a_0(980)$ model, we look more carefully into Eq. (30) and find that there are three contributions to the symmetry energy as

$$S(n_B) \equiv S_k(n_B) + S_\rho(n_B) + S_{a_0}(n_B), \tag{31}$$

where $S_k(n_B)$ is the kinetic contribution of the nucleon, and $S_\rho(n_B)$ and $S_{a_0}(n_B)$ are the contributions from ρ and $a_0(980)$ mesons, respectively. In the following discussion, we will focus on the results for $L_0 = 57.7$ MeV.

The kinetic contribution from the nucleons $S_k(n_B)$ is expressed as

$$S_k(n_B) \equiv \frac{n_B}{2}\left[\frac{(k_+^*)^2}{3\mu_+^* n_B}\right], \tag{32}$$

which accounts for the repulsion from the extra nucleon put into the symmetric matter. The density dependence of $S_k(n_B)$ is shown in Fig. 3. As expected, the kinetic contribution increases as the baryon number density increases. This is because higher baryon number density increases the repulsion between nucleons, and thus increases the energy of the matter.

The contribution from the $a_0(980)$ meson is expressed as

$$S_{a_0}(n_B) \equiv -\frac{n_B}{4}\frac{m_+^*}{\mu_+^*}\frac{\partial m_{+n}^*}{\partial n_I}\bigg|_{n_I=0}. \tag{33}$$

Figure 4 shows the S_{a_0} computed in the present model. We notice that S_{a_0} is negative and thus reduces the total symmetry energy $S(n_B)$. This is because $\frac{\partial m_{+n}^*}{\partial n_I}|_{n_I=0}$ is always positive as shown in Fig. 5. Intuitively, this can be understood from the dependence of m_{+n}^* on the mean field a given in Eq. (22). If we vary the mean field a, m_{+n}^* will also change correspondingly. However, the effective chemical potential μ_n^* is not dependent on the mean field a directly as we can see from Eq. (21). This change of the effective mass m_{+n}^* due to the mean field a leads to the change of the momentum of

TABLE V. $\lambda_{\omega\rho}$ of model with $a_0(980)$ meson and $\lambda_6' = 0$.

m_0 (MeV)	500	600	700	800	900
$L_0 = 40$ MeV	0.0127	0.0251	0.0761	0.2916	2.4595
$L_0 = 50$ MeV	0.0119	0.0221	0.0649	0.2415	1.9427
$L_0 = 60$ MeV	0.0110	0.0192	0.0537	0.1914	1.4259
$L_0 = 70$ MeV	0.0101	0.0162	0.0425	0.1413	0.9091
$L_0 = 80$ MeV	0.0092	0.0132	0.0313	0.0911	0.3923

TABLE VII. $\lambda_{\omega\rho}$ of model without $a_0(980)$ meson.

m_0 (MeV)	500	600	700	800	900
$L_0 = 40$ MeV	0.0554	0.0857	0.1695	0.4159	2.5186
$L_0 = 50$ MeV	0.0451	0.0671	0.1301	0.3153	1.8903
$L_0 = 60$ MeV	0.0348	0.0486	0.0907	0.2147	1.2619
$L_0 = 70$ MeV	0.0245	0.0301	0.0513	0.1140	0.6336
$L_0 = 80$ MeV	0.0142	0.0116	0.0120	0.0134	0.0052

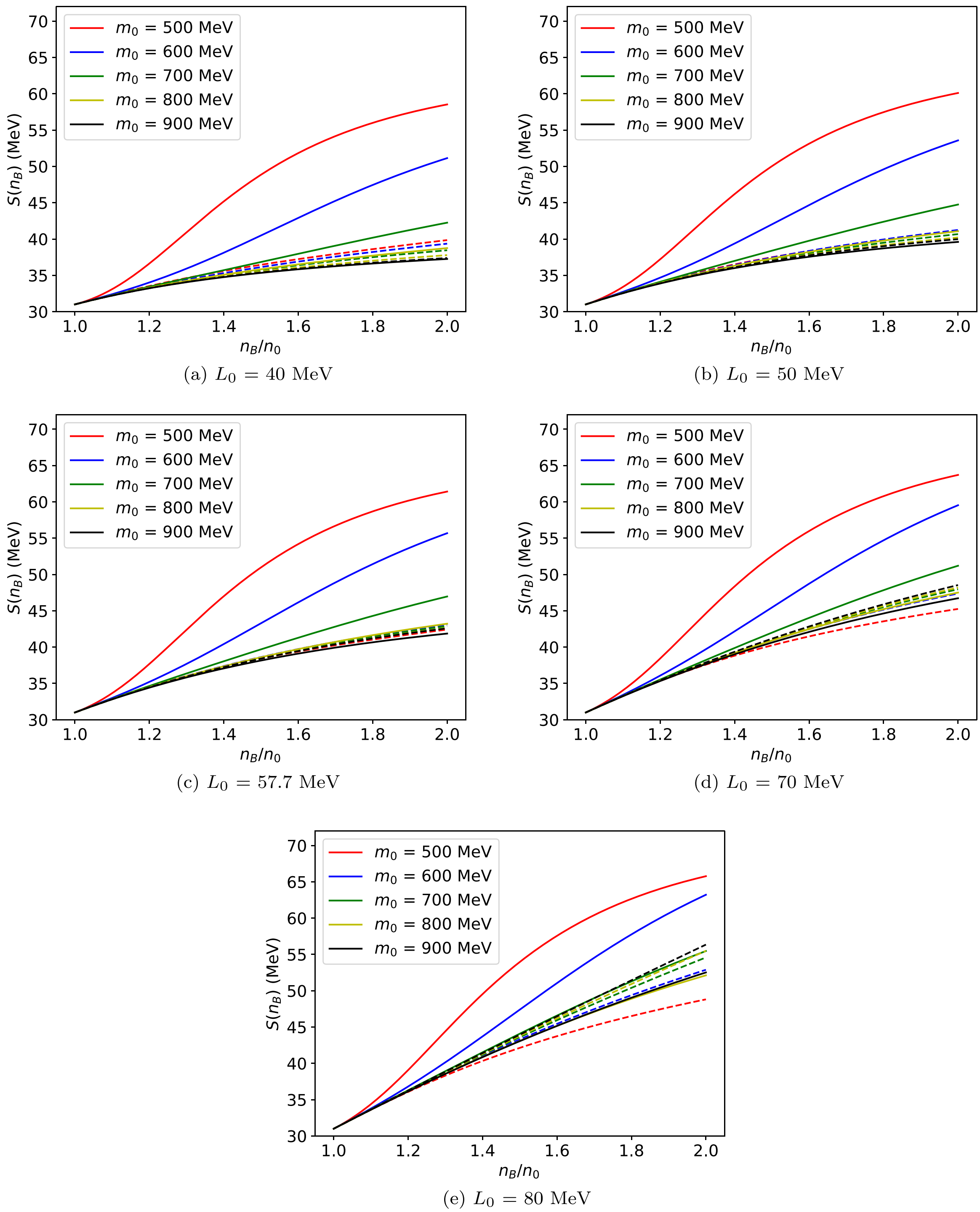

FIG. 2. Symmetry energy $S(n_B)$ for $m_0 = 500$–900 MeV and $L_0 = 40$–80 MeV. Solid curves represent the $S(n_B)$ of the model including $a_0(980)$ with $\lambda_6' = 0$, while dashed curves show the results of the model without $a_0(980)$.

the neutron $k_{+n} = \sqrt{(\mu_n^*)^2 - (m_{+n}^*)^2}$. When $n_I = n_p - n_n$ is increased for a fixed n_B, the density of the neutron n_n and thus the momentum k_{+n} is decreased. Accordingly, the effective mass of the neutron increases as n_I increase, causing a positive $\frac{\partial m_{+n}}{\partial n_I}|_{n_I=0}$. Therefore, the $a_0(980)$ meson contribution $S_{a_0}(n_B)$ reduces the total symmetry energy $S(n_B)$ in the present model. We also find that the $a_0(980)$ effect on the symmetry energy is stronger for smaller m_0. This is because the coupling constants of the $a_0(980)$ meson to the nucleon, g_1 and g_2, are larger for smaller m_0 as shown in Table I. As a result, the symmetry energy is enlarged by the $a_0(980)$ meson more when m_0 is smaller. In addition, we notice that the $a_0(980)$ effect on the symmetry energy is decreasing as the density increases since $\frac{\partial m_{+n}}{\partial n_I}|_{n_I=0}$ decreases.

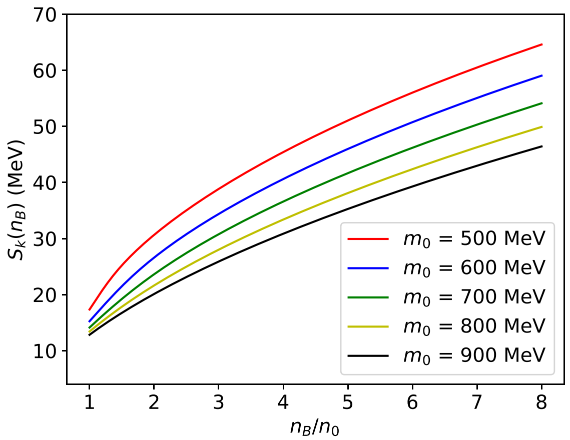

FIG. 3. Density dependence of $S_k(n_B)$ for $m_0 = 500$–900 MeV and $L_0 = 57.7$ MeV.

The third contribution comes from the ρ meson which is expressed as

$$S_\rho(n_B) \equiv \frac{n_B}{2}\left[\frac{(g_\rho/2)^2}{m_\rho^2 + \left(2\lambda_{\omega\rho} g_\omega^4 g_\rho^2 n_B^2/m_\omega^4\right)}\right]. \tag{34}$$

The density dependence of S_ρ is shown in Fig. 6. This shows that the contribution is always positive and thus provides repulsive force to the matter. We notice that the ω meson affects the symmetry energy through $2\lambda_{\omega\rho} g_\omega^4 g_\rho^2 n_B^2/m_\omega^4$ in the denominator. Since $\lambda_{\omega\rho} > 0$ as shown before, the ω-ρ mixing term always reduces the symmetry energy. In the case of large m_0 such as $m_0 = 900$ MeV, where the $a_0(980)$ meson effect is small, the softening effect of the $\lambda_{\omega\rho}$ term overrides the stiffening effect from the $a_0(980)$ meson. As a result, the symmetry energy $S(n_B)$ is reduced after the inclusion of the a_0 meson. A similar reduction of symmetry energy in the intermediate density region was also reported in Ref. [54] which includes both the scalar meson mixing and the vector meson mixing interactions in a RMF model with the presence of isovector-scalar meson.

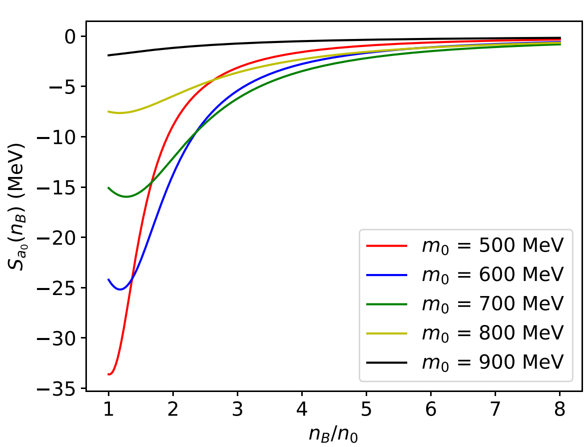

FIG. 4. Density dependence of $S_{a_0}(n_B)$ for $m_0 = 500$–900 MeV and $L_0 = 57.7$ MeV.

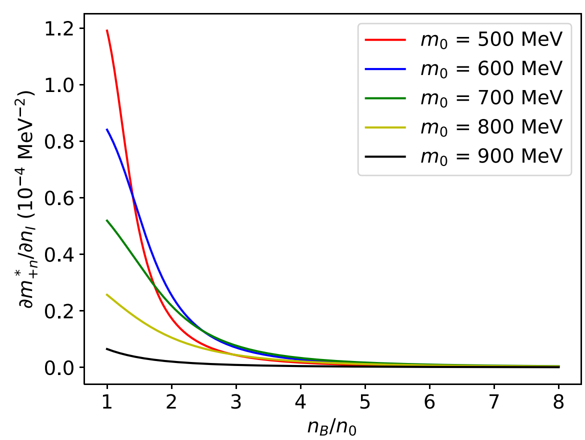

FIG. 5. Density dependence of $\frac{\partial m^*_{+n}}{\partial n_I}|_{n_I=0}$ for $m_0 = 500$–900 MeV and $L_0 = 57.7$ MeV.

Moreover, we observe in Fig. 6 that S_ρ is increasing with increasing n_B in the low-density region and is decreasing in the high-density region. This is understood as follows: In the low-density region, $m_\rho^2 \gg 2\lambda_{\omega\rho} g_\omega^4 g_\rho^2 n_B^2/m_\omega^4$ is satisfied which implies that the density dependence of $S(n_B)$ is determined by the prefactor n_B. In the high density region, on the other hand, the denominator is dominated by $2\lambda_{\omega\rho} g_\omega^4 g_\rho^2 n_B^2/m_\omega^4$, which leads to $S_\rho(n_B) \propto 1/n_B$.

Based on the above properties of three contributions, the symmetry energy can be understood as a result of the competition between the repulsive ρ meson interaction (modified by the ω-ρ mixing interaction) and the attractive $a_0(980)$ interaction, in addition to the kinetic contribution from the nucleons. On the other hand, in the model without an a_0 meson, only repulsive contributions exist. Since the symmetry energy at saturation density is fixed as $S_0 = 31$ MeV in both models with and without an $a_0(980)$ meson, the ρ meson coupling g_ρ is strengthened by the existence of the attractive $a_0(980)$ contribution in the model with a_0 comparing to the model without a_0. Actually, from Tables IV and VI it is clear that g_ρ is larger in the a_0 model than in the no-a_0 model for a fixed m_0 and L_0. In addition, g_ρ is larger as the Yukawa coupling

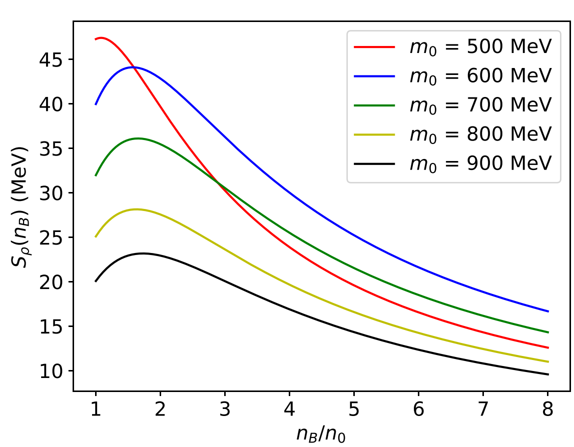

FIG. 6. Density dependence of $S_\rho(n_B)$ for $m_0 = 500$–900 MeV and $L_0 = 57.7$ MeV.

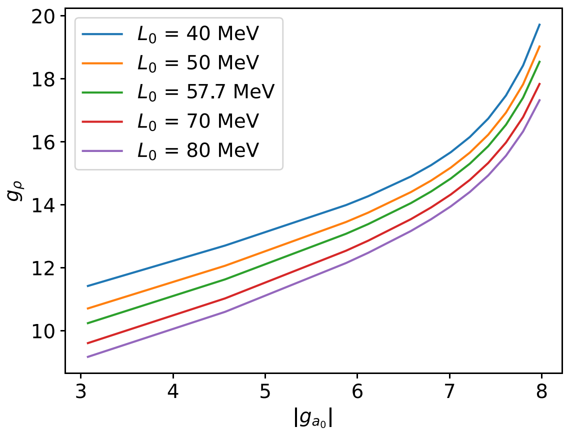

FIG. 7. Relation between g_ρ and $|g_{a_0NN}|$ for $L_0 = 57.7$ MeV.

of the a_0 meson $|g_{a_0NN}|$ increases as shown in Fig. 7. Since the ρ contribution S_ρ depends on n_B as shown in Eq. (34), the symmetry energy in the a_0 model increases with increasing density more rapidly than in the no-a_0 model. The difference between the a_0 model and the no-a_0 model becomes transparent for smaller m_0, since the Yukawa coupling of a_0 is larger for smaller m_0.

In addition, we investigate the effect of higher-order terms in the large N_c expansion for the six-point interaction on the symmetry energy by taking $\lambda_6' = \pm\lambda_6$. The results of the symmetry energies with different values of λ_6' are shown in Fig. 8. We can see that the difference between the symmetry energies for models with the same m_0 and L_0 is small, which indicates that the effect of λ_6' on the symmetry energy is small. Notice also that the difference becomes smaller for larger m_0, due to a smaller $a_0(980)$ effect.

At the end of this section, we compare our results of $S(2n_0)$ to the values obtained in other models in Fig. 9: Walecka-type RMF model with a_0 meson [54], extended Skyrme-Hartree-Fock model fitted with the PREX-II data [67], UrQMD transport model fitted with the ASY-EOS Collaborations data [68], and direct inversions of observed NS radii, tidal deformability, and maximum mass in the high-density EOS space [69]. This figure shows that the results from most parameter regions are consistent with those from other models. We expect that future experimental information for $S(2n_0)$ will further constrain the chiral invariant mass m_0.

V. EFFECT OF a_0(980) TO THE NEUTRON STAR PROPERTIES

In this section, we investigate how the neutron star properties are affected by the existence of the $a_0(980)$ meson. It is expected that $a_0(980)$ meson changes the neutron star properties, as a neutron star is highly asymmetric and thus should suffer net effect from isospin asymmetry. In the following, we obtain an EoS of neutron star matter (NSM) using the present PDM, which we use in the low-density region $n_B \leqslant 2n_0$, and construct a unified EoS using the interpolation method adopted in Refs. [33,38]. Then, we study the the effect of $a_0(980)$ to the M-R relation.

A. Neutron star matter EoS in the PDM

In the low-density region $n_B \leqslant 2n_0$, we use the present PDM to construct the EoS for NSM. In this work, we consider a electrically neutral cold neutron star in equilibrium. The hadronic thermodynamic potential $\Omega_{\rm NSM}$ is given by

$$\Omega_{\rm NSM} \equiv \Omega_H + \sum_{l=e,\mu} \Omega_l \,, \tag{35}$$

where we include the leptonic thermodynamic potentials Ω_l to account for electrons and muons. Notice that the mean fields are constrained by the stationary conditions

$$\left.\frac{\partial\Omega}{\partial\phi_i}\right|_{\phi_i} = 0 \,, \tag{36}$$

where $\phi_i = (\sigma, a, \omega, \rho)$ for the matter with $a_0(980)$, while $\phi_i = (\sigma, \omega, \rho)$ for matter without $a_0(980)$. Together with charge neutrality, we obtain $\Omega_{\rm NSM}$ and thus the pressure for the neutron star:

$$P_{\rm NSM} = -\Omega_{\rm NSM} \,. \tag{37}$$

The EoSs constructed with $a_0(980)$ meson are shown together with the EoSs without $a_0(980)$ meson in Fig. 10. We see that the EoSs for a fixed n_B are stiffened after the inclusion of the $a_0(980)$ meson. This is understood as follows: The inclusion of $a_0(980)$ strengthens the repulsive ρ meson effect to maintain the saturation properties, as mentioned in the previous section. The attractive a_0 effect decreases with increasing density, while the repulsive ρ meson effect increases. As a result, the pressure at a fixed n_B is larger when the $a_0(980)$ meson is included.

In Fig. 10, we also show the EoSs with $\lambda_6' = \pm\lambda_6$. This shows that the effect of λ_6' to the EoS is small in most of the cases. This is expected because the high-order interactions are suppressed in the larger N_c limit.

B. Unification of neutron star EoS

Following Refs. [33,38], we interpolate the EoS obtained from the present model in the low-density region $n_B \leqslant 2n_0$ and the one from the $SU(3)_L \times SU(3)_R$ NJL-type quark model for $n_B \geqslant 5n_0$, to construct the unified EoS exhibiting hadron-quark continuity. We think that it is not suitable to use the PDM in the higher density region since hyperons, which are not included in the present PDM, may appear at such a high density region. Here, we briefly summarize the way of interpolation. (See, for detail, Refs. [33,38].)

In the interpolating regime, the pressure P_I is expanded as a function of μ_B as

$$P_I(\mu_B) \equiv \sum_{i=0}^{5} c_i \mu_B^i \,, \tag{38}$$

where c_i are coefficients to be determined. This $P_I(\mu_B)$ is connected to the hadronic EoS $P_H(\mu_B)$ at $\mu_B = \mu_B^L$, where μ_B^L is the chemical potential corresponding to the density twice

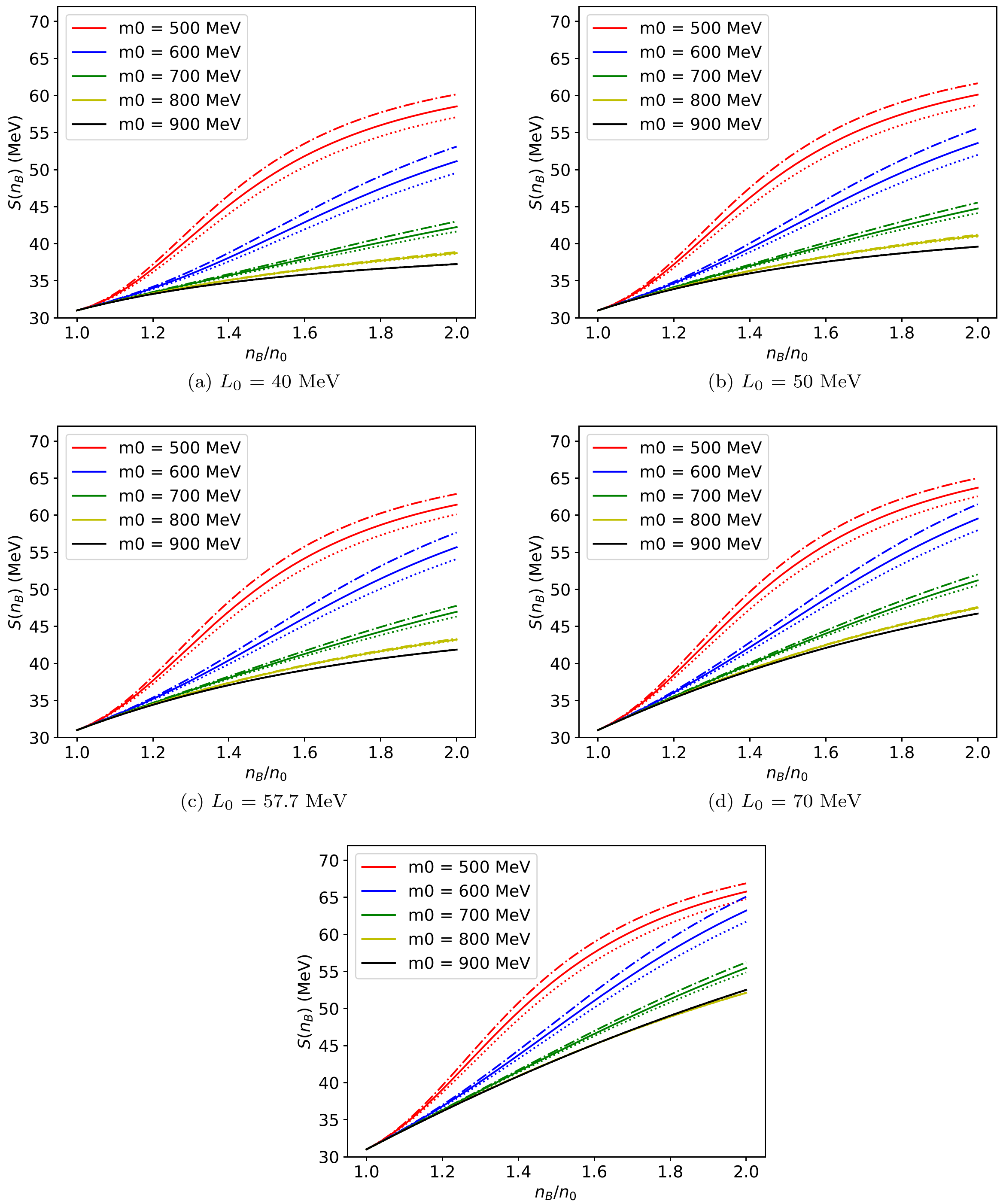

(a) $L_0 = 40$ MeV

(b) $L_0 = 50$ MeV

(c) $L_0 = 57.7$ MeV

(d) $L_0 = 70$ MeV

(e) $L_0 = 80$ MeV

FIG. 8. Density dependence of the symmetry energy $S(n_B)$ of the model including $a_0(980)$ meson for several choices of m_0 with $L_0 = 40$–80 MeV. Solid, dash-dotted, and dotted curves show the $S(n_B)$ with $\lambda_6' = 0$, λ_6, and $-\lambda_6$, respectively.

the normal nuclear density, $n_B = 2n_0$, by requiring

$$P_I(\mu_B = \mu_B^L) = P_H(\mu_B = \mu_B^L)\,,$$
$$\frac{\partial^n P_I}{\partial \mu_B^n}\bigg|_{\mu_B=\mu_B^L} = \frac{\partial^n P_H}{\partial \mu_B^n}\bigg|_{\mu_B=\mu_B^L}\,, \quad (n = 1, 2)\,. \tag{39}$$

Similarly, $P_I(\mu_B)$ is connected to $P_Q(\mu_B)$ constructed from the NJL-type quark model by requiring

$$\frac{\partial^n P_I}{\partial \mu_B^n}\bigg|_{\mu_B=\mu_B^H} = \frac{\partial^n P_Q}{\partial \mu_B^n}\bigg|_{\mu_B=\mu_B^H}\,, \quad (n = 0, 1, 2)\,, \tag{40}$$

where μ_B^H is the chemical potential corresponding to $n_B = 5n_0$. We accept the EoS as a physical one when the sound

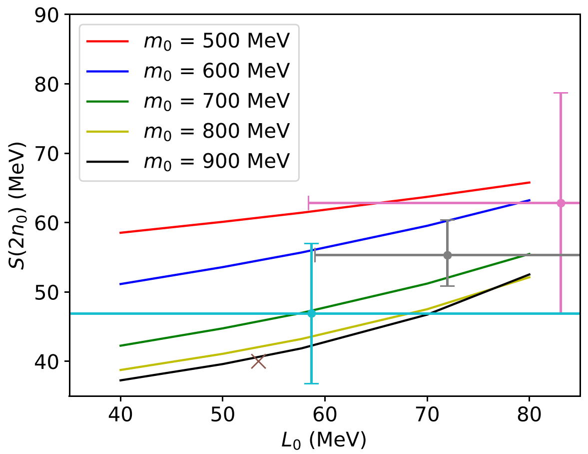

FIG. 9. Comparison of $S(2n_0)$ with other models: Refs. [54] (brown crosses), [67] (pink), [68] (grey), and [69] (cyan).

velocity c_s, calculated as

$$c_s^2 \equiv \frac{\partial P}{\partial \epsilon} = \frac{\partial P}{\partial \mu_B}\frac{\partial \mu_B}{\partial n_B}\frac{\partial n_B}{\partial \epsilon} = \frac{1}{\mu_B}\frac{n_B}{\frac{\partial^2 P}{\partial \mu_B^2}} , \tag{41}$$

is smaller than the speed of light

$$0 \leqslant c_s \leqslant 1 . \tag{42}$$

This requirement restricts the range of NJL parameters $(H/G, g_v/G)$, which are shown in Fig. 11. In the figure, the winter-colored squares and autumn-colored squares show the allowed parameters for the model with and without $a_0(980)$, respectively. This shows a positive correlation between H/G and g_v/G, which agrees with previous studies [33,37,38,41]. We also notice that the allowed NJL parameter sets of the a_0 model favor slightly larger g_v compared to the model without an $a_0(980)$ meson because the hadronic EoSs are slightly stiffened as shown in Fig. 10.

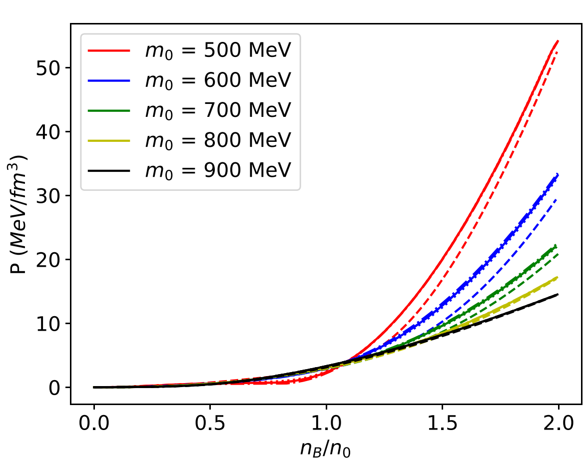

FIG. 10. Comparison of pressure of the NSM, $P_{\rm NSM}(n_B)$ with $a_0(980)$ (solid curves) and without $a_0(980)$ (dashed curves) for several values of m_0 with $L_0 = 57.7$ MeV. Dash-dotted and dotted curves show the EoS with $\lambda_6' = \lambda_6$ and $-\lambda_6$, respectively.

TABLE VIII. Summary of constraints of the chiral invariant mass m_0 for the models with different L_0. The unit of m_0 is in MeV.

	With a_0	Without a_0
$L_0 = 40$ MeV	$510 \lesssim m_0 \lesssim 830$	$500 \lesssim m_0 \lesssim 840$
$L_0 = 50$ MeV	$560 \lesssim m_0 \lesssim 840$	$520 \lesssim m_0 \lesssim 850$
$L_0 = 60$ MeV	$580 \lesssim m_0 \lesssim 860$	$540 \lesssim m_0 \lesssim 870$
$L_0 = 70$ MeV	$610 \lesssim m_0 \lesssim 890$	$570 \lesssim m_0 \lesssim 910$
$L_0 = 80$ MeV	$640 \lesssim m_0 \lesssim 940$	$610 \lesssim m_0 \lesssim 950$

Finally in this subsection, we show some typical examples of interpolated EoSs in Fig. 12 with the corresponding speed of sound in Fig. 13.

C. Mass-radius relation

In this subsection, we compute the M-R relation by solving the Tolman-Oppenheimer-Volkoff (TOV) equation [70,71], and comparing the results with the observational data.

We first examine how the existence of $a_0(980)$ affects to the M-R relation. In Fig. 14, we show some typical examples of the M-R relations computed with and without the existence of $a_0(980)$ for $m_0 = 600$, 700, and 800 MeV where $\lambda_6' = 0$ and $L_0 = 57.7$ MeV are taken. This figure clearly shows that inclusion of the $a_0(980)$ meson has increased the radius for the neutron stars with the mass of $0.5 \lesssim M/M_\odot \lesssim 2$, by the amount of $\lesssim 1$ km depending on the parameters. We see that the difference becomes smaller for larger m_0 similarly to the one for the symmetry energy. This is because the $a_0(980)$ meson couples to the matter weaker for large m_0. In addition, we observe that the $a_0(980)$ meson has little effect on the maximum mass, since the core of such a heavy neutron star includes the quark matter and the maximum mass is mainly determined by the parameters of the NJL-type quark model.

We also study the effect of high-order interaction in the large N_c limit to the M-R relation. Figure 15 shows the computed M-R relations of the models with different choices of λ_6'. As expected, we find that λ_6' has small effect on the M-R relation and changes the radius by only $\lesssim$0.5 km.

We compare the results to the observational constraints on neutron star mass and radius obtained from PSR J0030+0451 by [46], PSR J0740+6620 by [72], and GW170817 by [73], which restricts the value of the chiral invariant mass as

$$580 \text{ MeV} \lesssim m_0 \lesssim 860 \text{ MeV} \tag{43}$$

for $L_0 = 57.7$ MeV and $\lambda_6' = 0$. The constraint is increased by $\sim$200 MeV compared to the results of Refs. [37,38] considering the $U(1)_A$ anomaly. The constraints for different choices of L_0 are summarized in Table VIII. This shows that the effect of the a_0 meson increases the lower bound by about 10–40 MeV and reduces the upper bound by about 10–20 MeV. We note that, for $L_0 = 80$ MeV in the no-a_0 model, the saturation properties cannot be satisfied when $m_0 \gtrsim 960$ MeV.

In the present study, we used the interpolation density for PDM as $n_I^{\rm PDM} = 2n_0$ to avoid the direct consideration of hyperons. Here, we study the dependence of our results on the choice of $n_I^{\rm PDM}$ by taking $n_I^{\rm PDM} = 1.5n_0$ and $2.5n_0$. We find that, when the interpolation density of PDM is increased, the

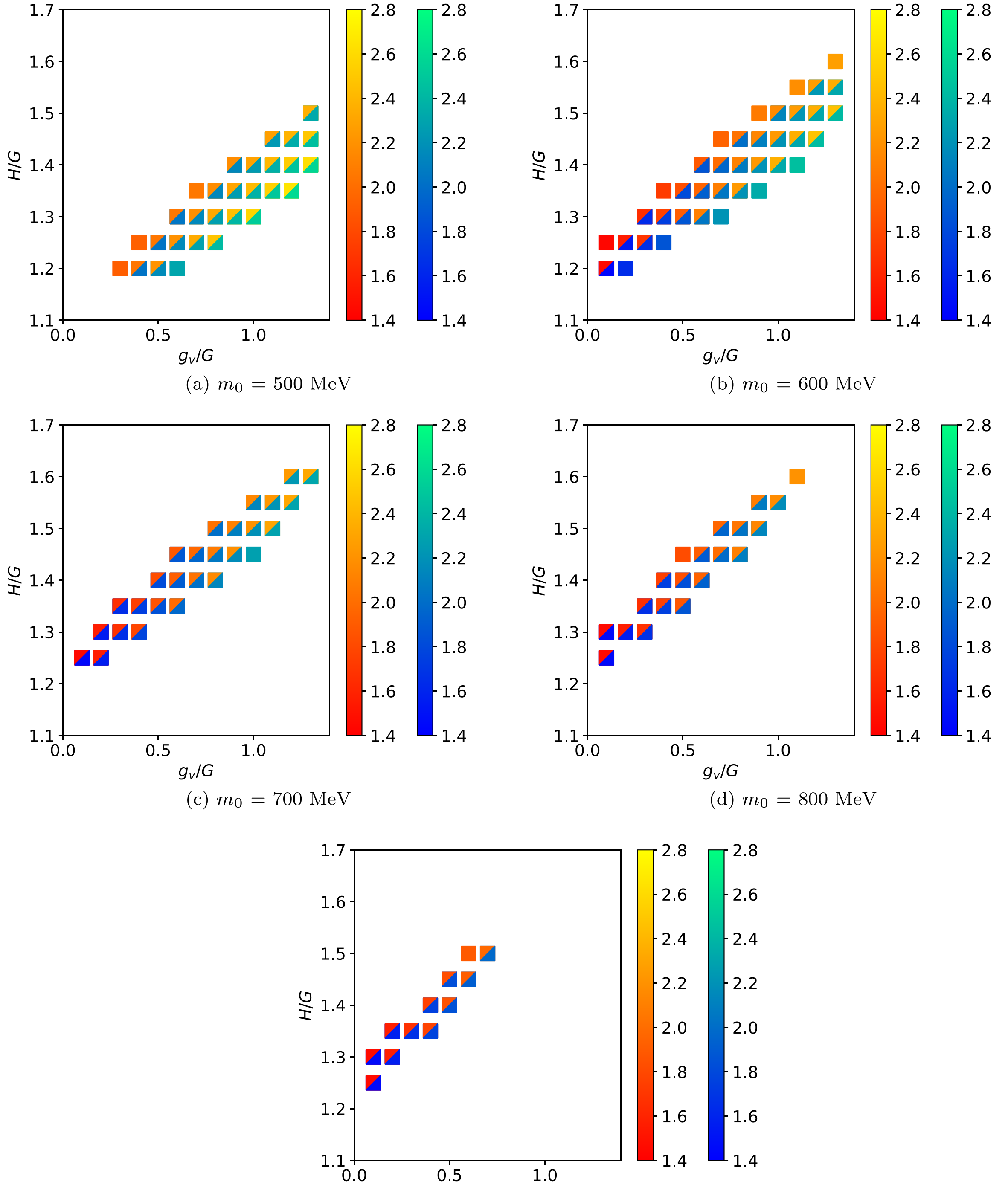

(a) $m_0 = 500$ MeV (b) $m_0 = 600$ MeV

(c) $m_0 = 700$ MeV (d) $m_0 = 800$ MeV

(e) $m_0 = 900$ MeV

FIG. 11. Allowed range of NJL parameters $(H/G, g_v/G)$ for several choices of m_0 with $L_0 = 57.7$ MeV, $\lambda_6' = 0$. ■ shows the allowed parameters for the model with $a_0(980)$, while ■ shows the allowed parameters for the model without $a_0(980)$. ◪ represents the parameters that are allowed for both of the models. The color indicates the maximum mass of the corresponding neutron star in the unit of solar mass.

allowed values of $(H/G, g_v/G)$ are narrowed down. Accordingly, decreasing the interpolating density from $n_I^{\mathrm{PDM}} = 2n_0$ to 1.5 n_0 reduces the lower limit of m_0 constraint of a_0 model with $L_0 = 57.7$ MeV by 20 MeV and increases the upper limit by 90 MeV, while increasing n_I^{PDM} from $2n_0$ to 2.5 n_0 does not change the lower limit of allowed m_0 and reduces the upper limit by 50 MeV. We think that it is not suitable to use a high interpolation density since the details of the hyperon appearance in a neutron star is not well known. Then the above results show that the dependence of the lower limit of m_0 is not so sensitive to the choice of the interpolating density. On the other hand, although the upper limit has some dependence, the stability of the nuclear matter at normal nuclear density requires $m_0 \lesssim 950$ MeV. Thus, the constraint to the chiral

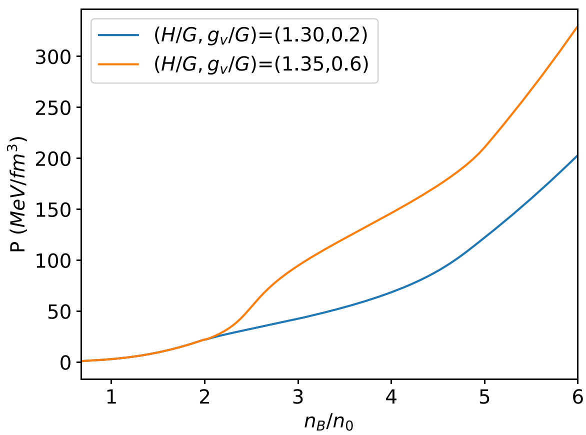

FIG. 12. Examples of interpolated pressure of neutron star matter with $a_0(980)$ for $m_0 = 700$ MeV, $L_0 = 57.7$ MeV, and $\lambda'_6 = 0$.

invariant mass is summarized as $m_0 \gtrsim 500$ MeV for small L_0, while $m_0 \gtrsim 600$ MeV for large L_0.

VI. SUMMARY AND DISCUSSIONS

We constructed a PDM with an a_0 meson based on the chiral $SU(2)_L \times SU(2)_R$ symmetry, and studied the effect of $a_0(980)$ on the symmetry energy and the neutron star properties. We showed that, for $m_0 \lesssim 800$ MeV, the symmetry energy in the density region $n_B \leqslant 2n_0$ is increased by the inclusion of an $a_0(980)$ meson, which leads to the stiffening of the EoS of neutron star matter resulting in an enlargement of the radius of the neutron star by about 1 km. This stiffening is understood as follows: The a_0 meson provides an attractive force to reduce the symmetry energy, which is balanced with the repulsive force by the ρ meson at the saturation density. Then, the repulsive force by the ρ meson is stronger in the a_0 model than in the no-a_0 model. Since the a_0 contribution decreases with increasing density while the ρ contribution increases, the symmetry energy increases more rapidly in the model with a_0 than the model without a_0. As a result, the symmetry energy is larger when the a_0 meson is included.

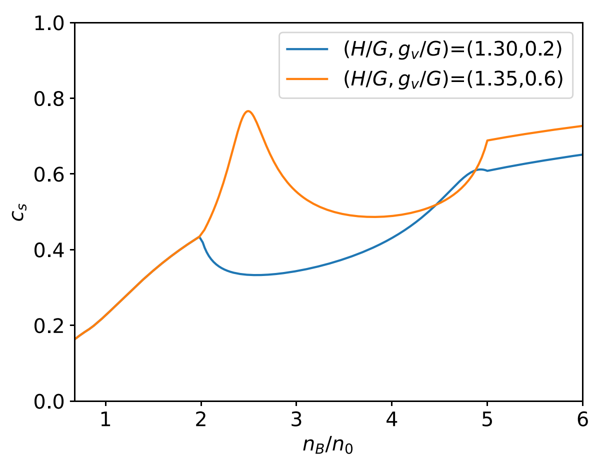

FIG. 13. Speed of sound c_s corresponding to the interpolated pressure in Fig. 12.

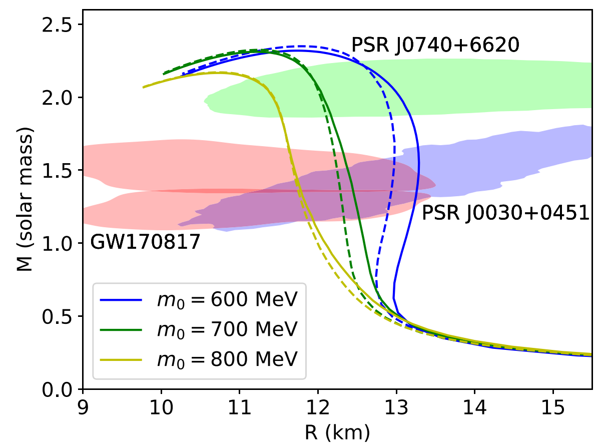

FIG. 14. M-R relations computed from models with and without the existence of $a_0(980)$ for different m_0 with $L_0 = 57.7$ MeV. Solid curves represent the M-R relations from the model with the $a_0(980)$ meson and dashed curves the ones of the model without $a_0(980)$. Parameters $(H/G, g_v/G)$ of the NJL-type quark model are chosen as to be the same for a specific m_0, (1.55,1.3) for $m_0 = 600$ MeV, (1.6,1.3) for $m_0 = 700$ MeV, and (1.55,1) for $m_0 = 800$ MeV, respectively.

Furthermore, since the Yukawa coupling of the a_0 meson to the nucleon is larger for smaller chiral invariant mass m_0, the stiffening effect of the a_0 meson is stronger for smaller m_0. We compared the resultant M-R relation to the neutron star observational data from PSR J0030+0451, PSR J0740+6620, and the gravitational wave event GW170817.

Including ambiguity of the interpolating density, below which the EoS is obtained from the present PDM, we conclude that the constraint to the chiral invariant mass is summarized as $m_0 \gtrsim 500$ MeV for small L_0, while $m_0 \gtrsim 600$ MeV for large L_0.

We also found that, for $m_0 = 900$ MeV, the symmetry energy is slightly reduced by including the effect of the a_0

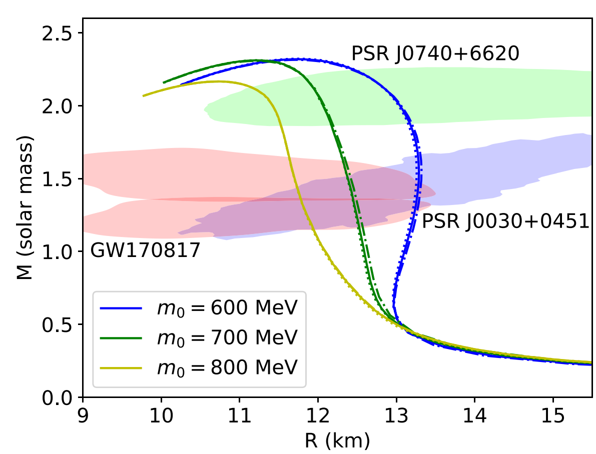

FIG. 15. M-R relations computed from models including $a_0(980)$ with different choices of λ'_6. Solid curves represent the results for $\lambda'_6 = 0$, dashed-dotted curves for $\lambda'_6 = +\lambda_6$, and dotted curves for $\lambda'_6 = -\lambda_6$. NJL parameters $(H/G, g_v/G)$ are chosen as (1.55,1.3) for $m_0 = 600$ MeV, (1.6,1.3) for $m_0 = 700$ MeV, and (1.55,1) for $m_0 = 800$ MeV. The slope parameter is fixed as $L_0 = 57.7$ MeV.

meson, due to the softening effect of ω-ρ mixing. This implies that the behavior of the symmetry energy for $n_B > n_0$ depends on the subtle balance among the effects of the a_0 meson attraction and the ρ meson repulsion combined with the ω-ρ mixing. We note that the softening effect by the a_0 meson is also reported in Refs. [54,55].

In the present analysis, we have included three terms for the six-point scalar meson interaction. As we showed, the effects from $tr[(M^\dagger M)^2]tr[M^\dagger M]$ and $\{tr[M^\dagger M]\}^3$, which are suppressed in the large N_c limit, are indeed small to the symmetry energy and the neutron star EoS. Therefore, these high-order effect may be ignored in the future to simplify the model.

ACKNOWLEDGMENTS

We would like to thank Ryota Yoda who performed primary analysis in his master thesis. This work was supported in part by JSPS KAKENHI Grants No. 20K03927 and No. 23H05439. T.M. was also supported by JST SPRING, Grant No. JPMJSP2125.

[1] C. DeTar and T. Kunihiro, Linear sigma model with parity doubling, Phys. Rev. D **39**, 2805 (1989).
[2] G. Aarts, C. Allton, S. Hands, B. Jäger, C. Praki, and J.-I. Skullerud, Nucleons and parity doubling across the deconfinement transition, Phys. Rev. D **92**, 014503 (2015).
[3] G. Aarts, C. Allton, D. De Boni, S. Hands, B. Jäger, C. Praki, and J.-I. Skullerud, Light baryons below and above the deconfinement transition: medium effects and parity doubling, J. High Energy Phys. 06 (2017) 034.
[4] J. Kim and S. H. Lee, Masses of hadrons in the chiral symmetry restored vacuum, Phys. Rev. D **105**, 014014 (2022).
[5] D. Jido, M. Oka, and A. Hosaka, Chiral symmetry of baryons, Prog. Theor. Phys. **106**, 873 (2001).
[6] T. Yamazaki and M. Harada, Chiral partner structure of light nucleons in an extended parity doublet model, Phys. Rev. D **99**, 034012 (2019).
[7] T. Hatsuda and M. Prakash, Parity doubling of the nucleon and first order chiral transition in dense matter, Phys. Lett. B **224**, 11 (1989).
[8] D. Zschiesche, L. Tolos, J. Schaffner-Bielich, and R. D. Pisarski, Cold, dense nuclear matter in a SU(2) parity doublet model, Phys. Rev. C **75**, 055202 (2007).
[9] V. Dexheimer, S. Schramm, and D. Zschiesche, Nuclear matter and neutron stars in a parity doublet model, Phys. Rev. C **77**, 025803 (2008).
[10] V. Dexheimer, G. Pagliara, L. Tolos, J. Schaffner-Bielich, and S. Schramm, Neutron stars within the SU(2) parity doublet model, Eur. Phys. J. A **38**, 105 (2008).
[11] C. Sasaki and I. Mishustin, Thermodynamics of dense hadronic matter in a parity doublet model, Phys. Rev. C **82**, 035204 (2010).
[12] C. Sasaki, H. K. Lee, W.-G. Paeng, and M. Rho, Conformal anomaly and the vector coupling in dense matter, Phys. Rev. D **84**, 034011 (2011).
[13] S. Gallas, F. Giacosa, and G. Pagliara, Nuclear matter within a dilatation-invariant parity doublet model: The role of the tetraquark at nonzero density, Nucl. Phys. A **872**, 13 (2011).
[14] W.-G. Paeng, H. K. Lee, M. Rho, and C. Sasaki, Dilaton-limit fixed point in hidden local symmetric parity doublet model, Phys. Rev. D **85**, 054022 (2012).
[15] J. Steinheimer, S. Schramm, and H. Stocker, The hadronic SU(3) parity doublet model for dense matter, its extension to quarks and the strange equation of state, Phys. Rev. C **84**, 045208 (2011).
[16] V. Dexheimer, J. Steinheimer, R. Negreiros, and S. Schramm, Hybrid stars in an SU(3) parity doublet model, Phys. Rev. C **87**, 015804 (2013).
[17] W.-G. Paeng, H. K. Lee, M. Rho, and C. Sasaki, Interplay between ω-nucleon interaction and nucleon mass in dense baryonic matter, Phys. Rev. D **88**, 105019 (2013).
[18] S. Benic, I. Mishustin, and C. Sasaki, Effective model for the QCD phase transitions at finite baryon density, Phys. Rev. D **91**, 125034 (2015).
[19] Y. Motohiro, Y. Kim, and M. Harada, Asymmetric nuclear matter in a parity doublet model with hidden local symmetry, Phys. Rev. C **92**, 025201 (2015); **95**, 059903(E) (2017).
[20] A. Mukherjee, J. Steinheimer, and S. Schramm, Higher-order baryon number susceptibilities: Interplay between the chiral and the nuclear liquid-gas transitions, Phys. Rev. C **96**, 025205 (2017).
[21] D. Suenaga, Examination of $N^*(1535)$ as a probe to observe the partial restoration of chiral symmetry in nuclear matter, Phys. Rev. C **97**, 045203 (2018).
[22] Y. Takeda, Y. Kim, and M. Harada, Catalysis of partial chiral symmetry restoration by Δ matter, Phys. Rev. C **97**, 065202 (2018).
[23] A. Mukherjee, S. Schramm, J. Steinheimer, and V. Dexheimer, The application of the quark-hadron chiral parity-doublet model to neutron star matter, Astron. Astrophys. **608**, A110 (2017).
[24] W.-G. Paeng, T. T. S. Kuo, H. K. Lee, Y.-L. Ma, and M. Rho, Scale-invariant hidden local symmetry, topology change, and dense baryonic matter. II., Phys. Rev. D **96**, 014031 (2017).
[25] M. Marczenko and C. Sasaki, Net-baryon number fluctuations in the hybrid quark-meson-nucleon model at finite density, Phys. Rev. D **97**, 036011 (2018).
[26] H. Abuki, Y. Takeda, and M. Harada, Dual chiral density waves in nuclear matter, EPJ Web Conf. **192**, 00020 (2018).
[27] M. Marczenko, D. Blaschke, K. Redlich, and C. Sasaki, Chiral symmetry restoration by parity doubling and the structure of neutron stars, Phys. Rev. D **98**, 103021 (2018).
[28] M. Marczenko, D. Blaschke, K. Redlich, and C. Sasaki, Parity doubling and the dense matter phase diagram under constraints from multi-messenger astronomy, Universe **5**, 180 (2019).
[29] T. Yamazaki and M. Harada, Constraint to chiral invariant masses of nucleons from GW170817 in an extended parity doublet model, Phys. Rev. C **100**, 025205 (2019).
[30] M. Harada and T. Yamazaki, Charmed mesons in nuclear matter based on chiral effective models, Jps Conf. Proc. **26**, 024001 (2019).
[31] M. Marczenko, D. Blaschke, K. Redlich, and C. Sasaki, Toward a unified equation of state for multi-messenger astronomy, Astron. Astrophys. **643**, A82 (2020).
[32] M. Harada, Dense nuclear matter based on a chiral model with parity doublet structure, in *Hadron Spectroscopy and Structure*,

edited by K. G. Feng and W. H. Liang (World Scientific, Singapore, 2020), pp. 661–666.

[33] T. Minamikawa, T. Kojo, and M. Harada, Quark-hadron crossover equations of state for neutron stars: Constraining the chiral invariant mass in a parity doublet model, Phys. Rev. C **103**, 045205 (2021).

[34] M. Marczenko, K. Redlich, and C. Sasaki, Reconciling multi-messenger constraints with chiral symmetry restoration, Astrophys. J. Lett. **925**, L23 (2022).

[35] T. Minamikawa, T. Kojo, and M. Harada, Chiral condensates for neutron stars in hadron-quark crossover: From a parity doublet nucleon model to a Nambu–Jona-Lasinio quark model, Phys. Rev. C **104**, 065201 (2021).

[36] M. Marczenko, K. Redlich, and C. Sasaki, Chiral symmetry restoration and Δ matter formation in neutron stars, Phys. Rev. D **105**, 103009 (2022).

[37] B. Gao, T. Minamikawa, T. Kojo, and M. Harada, Impacts of the $U(1)_A$ anomaly on nuclear and neutron star equation of state based on a parity doublet model, Phys. Rev. C **106**, 065205 (2022).

[38] T. Minamikawa, B. Gao, T. Kojo, and M. Harada, Chiral restoration of nucleons in neutron star matter: studies based on a parity doublet model, Symmetry **15**, 745 (2023).

[39] M. Marczenko, K. Redlich, and C. Sasaki, Fluctuations near the liquid-gas and chiral phase transitions in hadronic matter, Phys. Rev. D **107**, 054046 (2023).

[40] G. Baym, T. Hatsuda, T. Kojo, P. D. Powell, Y. Song, and T. Takatsuka, From hadrons to quarks in neutron stars: A review, Rep. Prog. Phys. **81**, 056902 (2018).

[41] G. Baym, S. Furusawa, T. Hatsuda, T. Kojo, and H. Togashi, New neutron star equation of state with quark–hadron crossover, Astrophys. J. **885**, 42 (2019).

[42] H. T. Cromartie *et al.* (NANOGrav Collaboration), Relativistic Shapiro delay measurements of an extremely massive millisecond pulsar, Nat. Astron. **4**, 72 (2019).

[43] B. P. Abbott *et al.* (LIGO Scientific, Virgo Collaboration), GW170817: observation of gravitational waves from a binary neutron star inspiral, Phys. Rev. Lett. **119**, 161101 (2017).

[44] B. P. Abbott *et al.* (LIGO Scientific, Virgo, Fermi GBM, INTEGRAL, IceCube, AstroSat Cadmium Zinc Telluride Imager Team, IPN, Insight-Hxmt, ANTARES, Swift, AGILE Team, 1M2H Team, Dark Energy Camera GW-EM, DES, DLT40, GRAWITA, Fermi-LAT, ATCA, ASKAP, Las Cumbres Observatory Group, OzGrav, DWF (Deeper Wider Faster Program), AST3, CAASTRO, VINROUGE, MASTER, J-GEM, GROWTH, JAGWAR, CaltechNRAO, TTU-NRAO, NuSTAR, Pan-STARRS, MAXI Team, TZAC Consortium, KU, Nordic Optical Telescope, ePESSTO, GROND, Texas Tech University, SALT Group, TOROS, BOOTES, MWA, CALET, IKI-GW Follow-up, H.E.S.S., LOFAR, LWA, HAWC, Pierre Auger, ALMA, Euro VLBI Team, Pi of Sky, Chandra Team at McGill University, DFN, ATLAS Telescopes, High Time Resolution Universe Survey, RIMAS, RATIR, SKA South Africa/MeerKAT Collaboration), Multi-messenger observations of a binary neutron star merger, Astrophys. J. Lett. **848**, L12 (2017).

[45] B. P. Abbott *et al.* (LIGO Scientific, Virgo Collaboration), GW170817: Measurements of neutron star radii and equation of state, Phys. Rev. Lett. **121**, 161101 (2018).

[46] M. Miller *et al.*, PSR J0030+0451 mass and radius from NICER data and implications for the properties of neutron star matter, Astrophys. J. Lett. **887**, L24 (2019).

[47] T. E. Riley *et al.*, A NICER view of PSR J0030+0451: Millisecond pulsar parameter estimation, Astrophys. J. Lett. **887**, L21 (2019).

[48] E. Fonseca *et al.*, Refined mass and geometric measurements of the high-mass PSR J0740+6620, Astrophys. J. Lett. **915**, L12 (2021).

[49] S. De, D. Finstad, J. M. Lattimer, D. A. Brown, E. Berger, and C. M. Biwer, Tidal deformabilities and radii of neutron stars from the observation of GW170817, Phys. Rev. Lett. **121**, 091102 (2018); **121**, 259902(E) (2018).

[50] D. Radice, A. Perego, F. Zappa, and S. Bernuzzi, GW170817: Joint constraint on the neutron star equation of state from multimessenger observations, Astrophys. J. Lett. **852**, L29 (2018).

[51] S. Kubis and M. Kutschera, Nuclear matter in relativistic mean field theory with isovector scalar meson, Phys. Lett. B **399**, 191 (1997).

[52] S. Kubis, M. Kutschera, and S. Stachniewicz, Neutron stars in relativistic mean field theory with isovector scalar meson, Acta Phys. Pol. B **29**, 809 (1998).

[53] T. Miyatsu, M.-K. Cheoun, and K. Saito, Asymmetric nuclear matter in relativistic mean-field models with isoscalar- and isovector-meson mixing, Astrophys. J. **929**, 82 (2022).

[54] F. Li, B.-J. Cai, Y. Zhou, W.-Z. Jiang, and L.-W. Chen, Effects of isoscalar- and isovector-scalar meson mixing on neutron star structure, Astrophys. J. **929**, 183 (2022).

[55] T. Miyatsu, M.-K. Cheoun, K. Kim, and K. Saito, Massive neutron stars with small radii in relativistic mean-field models optimized to nuclear ground states, arXiv:2209.02861.

[56] V. Thakur, R. Kumar, P. Kumar, V. Kumar, M. Kumar, C. Mondal, B. K. Agrawal, and S. K. Dhiman, Effects of an isovector scalar meson on the equation of state of dense matter within a relativistic mean field model, Phys. Rev. C **106**, 045806 (2022).

[57] B. Liu, H. Guo, M. D. Toro, and V. Greco, Neutron stars with isovector scalar correlations, Eur. Phys. J. A **25**, 293 (2005).

[58] A. Rabhi, C. Providência, and J. DaProvidência, Effect of the δ meson on the instabilities of nuclear matter under strong magnetic fields, Phys. Rev. C **80**, 025806 (2009).

[59] T. Gaitanos, M. D. Toro, S. Typel, V. Baran, C. Fuchs, V. Greco, and H. Wolter, On the Lorentz structure of the symmetry energy, Nucl. Phys. A **732**, 24 (2004).

[60] V. Greco, M. Colonna, M. Di Toro, and F. Matera, Collective modes of asymmetric nuclear matter in quantum hadrodynamics, Phys. Rev. C **67**, 015203 (2003).

[61] B. Liu, V. Greco, V. Baran, M. Colonna, and M. Di Toro, Asymmetric nuclear matter: The role of the isovector scalar channel, Phys. Rev. C **65**, 045201 (2002).

[62] S. Wang, H. F. Zhang, and J. M. Dong, Neutron star properties in density-dependent relativistic mean field theory with consideration of an isovector scalar meson, Phys. Rev. C **90**, 055801 (2014).

[63] X. Roca-Maza, X. Viñas, M. Centelles, P. Ring, and P. Schuck, Relativistic mean-field interaction with density-dependent meson-nucleon vertices based on microscopical calculations, Phys. Rev. C **84**, 054309 (2011).

[64] M. Bando, T. Kugo, and K. Yamawaki, Nonlinear realization and hidden local symmetries, Phys. Rep. **164**, 217 (1988).

[65] M. Harada and K. Yamawaki, Hidden local symmetry at loop: A new perspective of composite gauge boson and chiral phase transition, Phys. Rep. **381**, 1 (2003).
[66] B.-A. Li, B.-J. Cai, W.-J. Xie, and N.-B. Zhang, Progress in constraining nuclear symmetry energy using neutron star observables since GW170817, Universe **7**, 182 (2021).
[67] T.-G. Yue, L.-W. Chen, Z. Zhang, and Y. Zhou, Constraints on the symmetry energy from PREX-II in the multimessenger era, Phys. Rev. Res. **4**, L022054 (2022).
[68] P. Russotto, S. Gannon, S. Kupny, P. Lasko, L. Acosta, M. Adamczyk, A. Al-Ajlan, M. Al-Garawi, S. Al-Homaidhi, F. Amorini, L. Auditore, T. Aumann, Y. Ayyad, Z. Basrak, J. Benlliure, M. Boisjoli, K. Boretzky, J. Brzychczyk, A. Budzanowski, C. Caesar, G. Cardella, P. Cammarata, Z. Chajecki, M. Chartier, A. Chbihi, M. Colonna, M. D. Cozma, B. Czech, E. De Filippo, M. Di Toro, M. Famiano, I. Gašparić, L. Grassi, C. Guazzoni, P. Guazzoni, M. Heil, L. Heilborn, R. Introzzi, T. Isobe, K. Kezzar, M. Kiš, A. Krasznahorkay, N. Kurz, E. La Guidara, G. Lanzalone, A. Le Fèvre, Y. Leifels, R. C. Lemmon, Q. F. Li, I. Lombardo, J. Łukasik, W. G. Lynch, P. Marini, Z. Matthews, L. May, T. Minniti, M. Mostazo, A. Pagano, E. V. Pagano, M. Papa, P. Pawłowski, S. Pirrone, G. Politi, F. Porto, W. Reviol, F. Riccio, F. Rizzo, E. Rosato, D. Rossi, S. Santoro, D. G. Sarantites, H. Simon, I. Skwirczynska, Z. Sosin, L. Stuhl, W. Trautmann, A. Trifirò, M. Trimarchi, M. B. Tsang, G. Verde, M. Veselsky, M. Vigilante, Y. Wang, A. Wieloch, P. Wigg, J. Winkelbauer, H. H. Wolter, P. Wu, S. Yennello, P. Zambon, L. Zetta, and M. Zoric, Results of the ASY-EOS experiment at GSI: The symmetry energy at suprasaturation density, Phys. Rev. C **94**, 034608 (2016).
[69] N.-B. Zhang and B.-A. Li, Extracting nuclear symmetry energies at high densities from observations of neutron stars and gravitational waves, Eur. Phys. J. A **55**, 39 (2019).
[70] R. C. Tolman, Static solutions of Einstein's field equations for spheres of fluid, Phys. Rev. **55**, 364 (1939).
[71] J. R. Oppenheimer and G. M. Volkoff, On massive neutron cores, Phys. Rev. **55**, 374 (1939).
[72] M. C. Miller *et al.*, The radius of PSR j0740+6620 from nicer and XMM-Newton data, Astrophys. J. Lett. **918**, L28 (2021).
[73] B. P. Abbott *et al.*, Properties of the binary neutron star merger GW170817, Phys. Rev. X **9**, 011001 (2019).